Chemical Engineering Science 239 (2021) 116602

Contents lists available at ScienceDirect

Chemical Engineering Science

journal homepage: www.elsevier.com/locate/ces

Multi-reaction kinetic modeling for the peroxidase–aldolase cascade synthesis of a D-fagomine precursor

Gerard Masdeu [a,*], Zvjezdana Findrik Blažević [b], Slavko Kralj [c,d], Darko Makovec [c], Josep López-Santín [a], Gregorio Álvaro [a]

[a] Department of Chemical, Biological and Environmental Engineering, Universitat Autònoma de Barcelona, Bellaterra, Spain
[b] Faculty of Chemical Engineering and Technology, University of Zagreb, Zagreb, Croatia
[c] Department for Materials Synthesis, Jožef Stefan Institute, Ljubljana, Slovenia
[d] Faculty of Pharmacy, University of Ljubljana, Ljubljana, Slovenia

HIGHLIGHTS

- Multi-enzymatic reaction cascade evaluation for the synthesis of iminocyclitols.
- A complex system composed of seven distinct reaction and two enzyme inactivation.
- Kinetic modeling for elucidation of reaction mechanism.
- Cross-inhibition and inactivation in peroxidase/aldolase reactions.
- High improvement in reaction productivity through process intensification.

GRAPHICAL ABSTRACT

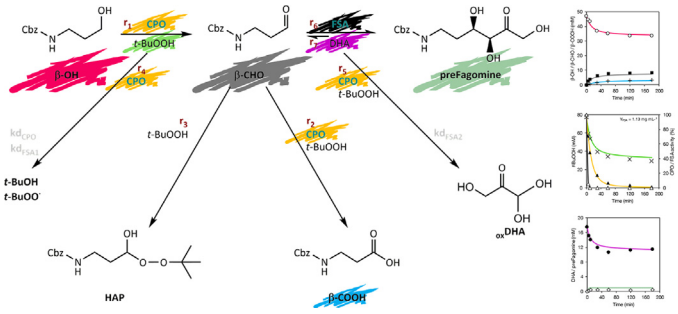

ARTICLE INFO

Article history:
Received 20 February 2021
Accepted 19 March 2021
Available online 22 March 2021

Keywords:
Enzymatic reaction cascade
Peroxidase
Aldolase
D-fagomine
Kinetic modeling

ABSTRACT

The feasibility of a peroxidase–aldolase cascade reaction for the synthesis of therapeutically-valuable iminocyclitols is discussed herein. A two-enzyme system consisting of chloroperoxidase (CPO) and D-fructose-6-phosphate aldolase (FSA) was evaluated for the synthesis of a D-fagomine precursor (preFagomine) from a *N*-Cbz-3-aminopropanol. An in-depth, systematic, step-by-step kinetic modeling of seven reactions and two inactivation decays was proposed to elucidate the reaction mechanism, prepare suitable stabilized biocatalysts, and find the optimal conditions for its application. The model described accurately the data and predicted the outcome at different experimental conditions. The inactivation of FSA caused by CPO was identified as the main bottleneck in the reaction. A two-step reaction approach and the use of immobilized enzymes on magnetic nanoparticle clusters and functionalized agarose carriers increased the stability of FSA, with an 1839-fold higher preFagomine formation per mol of enzyme in comparison to a one-pot reaction using soluble enzymes.

1. Introduction

Iminocyclitols, also referred to as iminosugars, are carbohydrate analogs in which a nitrogen atom has replaced the endocyclic oxygen. These compounds are inhibitors of glycosidases with enormous therapeutic potential in many diseases by altering the glycosylation or catabolism of glycoproteins (Calveras et al.,

Abbreviations: CPO, chloroperoxidase; FSA, D-fructose-6-phosphate aldolase; preFagomine, (3S,4R)-6-[(benzyloxycarbonyl)amino]-5,6-dideoxyhex-2-ulose); DHA, dihydroxyacetone; β-OH, *N*-Cbz-3-aminopropanol; β-CHO, *N*-Cbz-3-aminopropanal; β-COOH, *N*-Cbz-3-aminopropanoic acid; *t*-BuOOH, *t*-butyl hydroperoxide; mNC, magnetic nanoparticle clusters; MANA-agarose, Monoaminoethyl-N-aminoethyl agarose; CoIDA-agarose, cobalt-iminodiacetic acid-agarose.

* Corresponding author.
E-mail address: gemasdeu@gmail.com (G. Masdeu).

https://doi.org/10.1016/j.ces.2021.116602
0009-2509/

2009; Gloster et al., 2007; Stütz, 1999; Whalen and Wong, 2006). One valuable iminocyclitol is D-fagomine (Gómez et al., 2012; Hereu et al., 2019; Koyama and Sakamura, 1974; Pearson et al., 2005), which is a nutraceutical that may be used in diabetes cases to prevent the digestion and absorption of carbohydrates (Fan et al., 1999; Nojima et al., 1998; Taniguchi et al., 1998). Chemical syntheses of D-fagomine with carbohydrate precursors as starting materials usually involve cumbersome protection-deprotection reactions, achieving moderate isolated yields (Fleet et al., 1987; Goujon et al., 2005; Kumari et al., 2009; Pandey and Kapur, 2000); the synthesis from amino aldehydes is also described with final yields below 15% (Banba et al., 2001). Alternatively, a D-fagomine precursor (preFagomine, (3S,4R)-6-[(benzyloxycarbonyl)amino]-5,6-dideoxyhex-2-ulose) has been synthesized with 89% of isolated yield through stereoselective aldol addition of dihydroxyacetone (DHA) to *N*-Cbz-3-aminopropanal (β-CHO) (Fig. 1b) (Castillo et al., 2006). The aldol addition was catalyzed by D-fructose-6-phosphate aldolase (FSA, EC 4.1.2.-), a class I aldolase from *E. coli* that is not dependent on phosphorylated donor substrates. This substrate promiscuity has allowed many syntheses of iminocyclitols, which have been assayed against a panel of glycosidases (Herna et al., 2019; Sugiyama et al., 2007). Several FSA genetic variants with modified substrate specificity are described elsewhere (Gutierrez et al., 2011; Szekrenyi et al., 2014).

The chemical synthesis of the protected amino aldehydes is generally achieved with low selectivity and high cost of oxidizing agents. Transition metals are commonly used in these reactions, making the process environmentally unsuitable (Lenoir, 2006). The oxidation of alcohols to aldehydes is hence advantageous to be performed via an enzymatic process. In previous work, the oxidation of *N*-Cbz-3-aminopropanol (β-OH). to β-CHO was catalyzed by chloroperoxidase from *Caldariomyces fumago* (CPO, EC 1.11.1.10), with nearly full substrate conversion but only 18% selectivity towards the aldehyde, which could be increased by coupling the FSA reaction (Fig. 1a) (Masdeu et al., 2016a). A peroxide (hydrogen peroxide or t-butyl hydroperoxide, *t*-BuOOH) was used as a co-substrate, instead of the expensive cofactors required by dehydrogenases (Andersson and Wolfenden, 1982; Rodriguez-Hinestroza et al., 2017; Shaw and Hager, 1961; Sudar et al., 2015). Peroxides or derivate radical species, however, may cause a rapid inactivation of CPO probably by heme group destruction (Andersson et al., 2000; Ayala et al., 2011; Chamulitrat et al., 1989; Park and Clark, 2006; Shevelkova and Ryabov, 1996), similarly to the activity loss of dehydrogenases initiated by the supply of oxygen in the reactions (Sudar et al., 2021).

The aim of the present research is the evaluation of the feasibility of a two-reaction coupling employing CPO and FSA for the synthesis of preFagomine using β-OH, DHA and peroxide as starting materials. The elucidation of the reaction mechanism of both reactions is crucial for the determination of the initial reaction conditions for its application: the reaction buffer and pH, the type of peroxide, and the concentration of the substrates. Enzyme stability, side reactions (e.g. the formation of hydroxy peroxy intermediates) (Masdeu et al., 2016b) and substrate/product inhibitions may also alter both CPO and FSA catalytic rates (Robertson, 2005). The immobilization of both enzymes into agarose particles and magnetic nanoparticle clusters has been previously reported showing increased stability with corresponding higher conversion rates: CPO was immobilized on amino-functionalized agarose (Pešić et al., 2012) and magnetic nanoparticle clusters (mNC) (Masdeu et al., 2018), and FSA has been recently attached to both cobalt-iminodiacetic acid-agarose (CoIDA-agarose) and mNC (Masdeu et al., 2021).

The evaluation of the CPO/FSA reaction will be addressed through (i) kinetic modelling and (ii) process intensification. (i) The development of a mathematical kinetic model of the system enables process optimization and give insight into the relationship among the process variables: degradation of peroxide, chemical reaction, amino aldehyde oxidation, alcohol oxidation, DHA oxidation, aldol addition, and retroaldol addition. (ii) The optimal operating strategy of a complex system is approximated to maximize the reaction rates and product yield, while minimizing the formation of side products. In the case of a multi-enzyme system, a decomposition of the whole system on individual reaction steps is required for the model formulation and understanding of each individual reaction separately.

2. Materials and methods

2.1. Materials

β-OH, β-CHO, *N*-Cbz-3-aminopropanoic acid (β-COOH), *t*-BuOOH (70 wt% in H_2O), H_2O_2 (30 wt% in H_2O), 2,4-Dinitrophenylhydrazine phosphoric acid solution (DNPH), α-glycerophosphate dehydrogenase–triosephosphate isomerase (GPD/TPI), fructose-6-phosphate (F6P), D-glyceraldehyde-3-phosphate (G3P), NADH, *N*-(3-dimethylaminopropyl)-*N*'-ethylcarbodiimide (CDI), (3-aminopropyl)triethoxysilane, and ethylenediamine were purchased from Sigma Aldrich. 1,1-dimethyl-4-chloro-3,5-cyclohexadione (MCD) (Fluka), (Hydroxy(polyethyleneoxy)propyl) triethoxysilane (Gelest), 10% cross-linked agarose beads and high-density metal-chelated supports (20–40 μmol divalent metal ml^{-1}) with iminodiacetic acid for metal chelation (IDA-agarose) (Agarose Bead Technologies) were used. Iron (III) sulfate hydrate, iron (II) sulfate heptahydrate, citric acid, tetraethoxysilane (TEOS), NH_4OH, and DHA were supplied by Alfa Aesar.

CPO from *C. fumago* was purchased from Chirazyme Labs (42 KDa, 1400 U $mg^{-1}_{protein}$). Recombinant His-tagged FSA A129S (selected due to its high reactivity towards DHA) (Castillo et al., 2010; Sudar et al., 2013b) was produced in high-cell density fed-batch *Escherichia coli* BL21 (DE3) cell cultures by a modified protocol described elsewhere (Calleja et al., 2016). Plasmid pET22-fsaA was generously supplied by Dr. Clapés from Biotransformation and Bioactive Molecules Group (IQAC-CSIC, Barcelona). The enzyme was purified by (cobalt-chelated) affinity chromatography with a specific activity was 15.0 U $mg^{-1}_{protein}$ (257 KDa).

2.2. Preparation of immobilization carriers

Functionalized agarose supports were synthesized by previously described protocols: Monoaminoethyl-*N*-aminoethyl

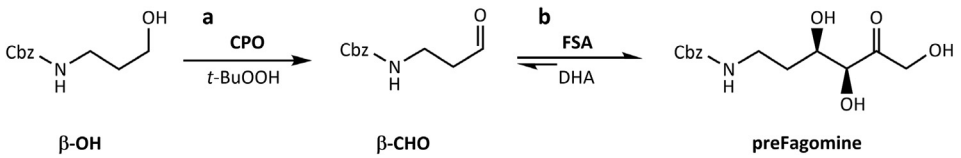

Fig. 1. Schematic representation of the enzymatic synthesis of preFagomine: (**a**) β-OH oxidation catalyzed by CPO using t-BuOOH. (**b**) DHA aldol addition to β-CHO catalyzed by FSA.

(MANA) agarose was prepared from 10% cross-linked agarose gels (Fernandez-Lafuente et al., 1993; Guisán, 1988), and CoIDA-agarose was prepared from IDA-agarose gels using cobalt chloride (Ardao et al., 2006).

mNC was obtained by the self-assembly of primary maghemite (γ-Fe_2O_3) nanoparticles followed by a coating of the magnetic cluster with a layer of silica (Kralj et al., 2010; Kralj and Makovec, 2015; Tadic et al., 2014). To functionalize and ensure the colloidal stability of the nanocomposite, silica-coated mNC was grafted with a mixed layer of silane molecules: ~83 mol. % (3-aminopropyl)triethoxysilane, and ~17 mol. % of the silane-PEG for the additional steric stabilization of suspensions (Kralj et al., 2011; Masdeu et al., 2018). Functionalized mNC are fully characterized and also commercially available by Nanos SCI company under trademark iNANOvative™.

2.3. Enzymatic activity assays

The activity of CPO was spectrophotometrically determined by the chlorination of MCD (ε_{278} = 12.2 mM^{-1} cm^{-1}) (Toti et al., 2005) to dichlorodimedone (DCD), according to the method of Hager and Morris (Morris and Hager, 1966). The enzymatic assay contained 0.1 M potassium phosphate buffer of pH 2.75, 0.16 mM MCD, 20 mM KCl, 2 mM hydrogen peroxide, and 50 μL of enzyme sample in a total volume of 1 ml (100 μL in 2 ml for immobilized derivatives). The absorbance at 278 nm was monitored at 25 °C using a Cary 50 Bio UV–Visible Spectrophotometer (Varian) by duplicate measurements. One activity unit (U) of CPO is defined as the amount of enzyme required for the conversion of 1 μmol of MCD per minute.

The activity of FSA was determined by a three-enzyme reaction described in the literature (Schürmann and Sprenger, 2001). The mixture for the enzymatic assay contained 5 mM F6P, 0.1 mM NADH, 50 mM imidazole, 10 U ml^{-1} of GPD-TPI, and 50 μL of the sample with FSA, in a total volume of 1 ml (100 μL in 2 ml volume for immobilized derivatives). FSA activity was monitored by the decrease at A_{340} due to the conversion of NADH to NAD^+ (ε_{340} = 6.2 mM^{-1} cm^{-1}) at 30 °C by duplicate measurements. 1 U of FSA activity is defined as the amount of enzyme required for the conversion of 1 μmol of F6P per minute. In the case of FSA bound to mNC-FSA, the activity was not quantified by absorption kinetics due to method sensitivity but using the aldol addition of DHA to β-CHO monitoring preFagomine by HPLC analysis (Masdeu et al., 2021). The immobilized enzyme (50 μL) was added to 950 μL of the reaction mixture, containing 40 mM β-CHO and 100 mM DHA in 50 mM HEPES (pH 8.0). The reaction was left for 90 min at 30 °C, 1000 rpm, and stopped by acidification to pH 2.5.

2.4. Enzyme immobilization

Native CPO was immobilized onto MANA-agarose (CPO-MANA-agarose) according to our previous method (Pešić et al., 2012). Briefly, MANA-agarose (50 mg) was mixed with CPO (764 U) in 1 ml of 10 mM sodium phosphate buffer (pH 5.0) at 25 °C for 15 min, and CDI (50 mM) was added for covalent immobilization. After 3 h, 1 M NaCl was incubated for an additional hour to avoid the ionic interactions. CPO was also immobilized onto mNC-NH_2 (mNC-NH_2-CPO) by prior modification of the surface of the enzyme (Masdeu et al., 2018). The sugar moieties on the surface of the enzyme (232 U ml^{-1}) were oxidized with 25 mM $NaIO_4$ in 0.5 ml of 50 mM phosphate buffer (pH 5.0) for 60 min. 50 mM propylene glycol was added to terminate the reaction. A colloidal suspension of mNC-NH_2 (50 mg) was mixed ™) with oxidized CPO (500 U) in 1 ml of 10 mM phosphate buffer (pH 5.0) at 25 °C for 2 h, followed by the addition of $NaBH_4$ (0.1 mg ml^{-1}) to reduce the formed Schiff base for 30 min. 1 M NaCl was added to avoid non-specific electrostatic interactions. As designed for reaction purposes, both derivatives had a final activity of 6.25 U mg^{-1} (CPO-MANA-agarose and mNC-NH_2-CPO retained activities of 40.9 and 62.5%, respectively).

The preparations of FSA-CoIDA-agarose and mNC-NH_2-FSA are fully described in our recent work (Masdeu et al., 2021). FSA (0.60 U) was immobilized on CoIDA-agarose (50 mg) for 30 min in 50 mM sodium phosphate buffer with 0.3 M NaCl and 20 mM imidazole, at pH 8.0 and 25 °C in a total volume of 1 ml. In parallel, 2.0 U FSA was immobilized onto 50 mg mNC-NH_2 in 10 mM phosphate buffer (pH 5.0), at 25 °C, and stirred at 1000 rpm. After 1-hour incubation, 5 mM CDI was added for 3 h to form the covalent bond between FSA and mNC-NH_2. Finally, 0.5 M NaCl was used to avoid non-covalent interactions. For reaction purposes, both derivatives had a final activity of 11.6 mU mg^{-1} (FSA-CoIDA-agarose and mNC-NH_2-FSA retained activities of 96.4 and 29.1%, respectively).

Final immobilized derivatives were washed with buffer, the volume was set to 0.3 ml, and they were immediately used for the reaction.

2.5. HPLC analysis

β-OH, β-CHO, β-COOH, *t*-BuOOH, and preFagomine were quantified by HPLC (Dionex UltiMate 3000 with variable wavelength detector) analysis using a CORTECS (Waters) C18 + 4.6 × 150 mm (2.7 μm) column. Reaction samples were dissolved in acetonitrile (MeCN) and analyzed by injecting 15 μL at a flow rate of 0.7 ml min^{-1}, 30 °C. The solvent system consisted of mobile phase A –0.1% (v/v) TFA in H_2O– and B –0.095% (v/v) TFA in MeCN/H_2O 4:1 (v/v)–. Samples were eluted using a gradient from 5 to 28.5% B in 0.5 min, and an isocratic elution at 28.5% B over 15 min (λ = 254 nm). For the quantification of DHA, sample derivatization was required before chromatography. DNPH derivatization was performed following a described protocol (Ferioli et al., 1995) 30 μL of DHA (0–2 mM) was mixed with 30 μL of a stock solution of DNPH (0.2 M) for 60 min; 180 μL of sodium acetate (3 M, pH 9.0) was added to stop the reaction. The derivatized compound was extracted into an organic phase using 240 μL of MeCN, and the HPLC analysis was performed eluting the samples with an isocratic method at 50% B for 2 min, followed by a gradient from 50 to 65% B over 5 min (λ = 260 nm). Prior calibration with standards of known concentration was used for quantitative analysis. The standard deviation was calculated from measurements performed by duplicate. In addition, the structures of preFagomine and oxidized DHA ($_{ox}$DHA) were characterized by HPLC-MS analysis (Figure S1, S2).

2.6. Mathematical model and kinetic parameters estimation

Reaction rates (**r**) were named according to the corresponding reaction (**R**) (Eqs. (1)–(19); nomenclature is revised in Supporting Information, SI section 3.1): $\mathbf{R_1}$ is the CPO-catalyzed β-OH oxidation to β-CHO, which can be further oxidized to β-COOH by the same enzyme and peroxide ($\mathbf{R_2}$). $\mathbf{R_3}$ represents the chemical reaction aldehyde-peroxide leading to the hydroxy alkyl peroxide (HAP) described in previous work (Masdeu et al., 2016a). $\mathbf{R_4}$ is the degradation of *t*-BuOOH by CPO that renders *tert*-butyl alcohol (*t*-BuOH) and a radical (*t*-$BuOO^{\cdot}$), as previously reported elsewhere (Chamulitrat et al., 1989). $\mathbf{R_5}$ states for the oxidation of DHA catalyzed by CPO leading to $_{ox}$DHA. $\mathbf{R_6}$ and $\mathbf{R_7}$ are the aldol and retroaldol additions by FSA.

The enzyme inactivation was simplified to a first-order decay. kd_{CPO} is the inactivation rate constant of CPO in presence of *t*-BuOOH; kd_{FSA1} is the inactivation rate of FSA caused by CPO and *t*-BuOOH; kd_{FSA2} is the FSA inactivation rate caused by CPO, DHA and *t*-BuOOH. The stoichiometry and mass balances from all reactions are:

$$R_1: \ \beta OH + t\text{BuOOH} \underset{\text{CPO}}{\rightarrow} \beta CHO + t\text{BuOH} \quad (1)$$

$$R_2: \ \beta CHO + t\text{BuOOH} \underset{\text{CPO}}{\rightarrow} \beta COOH + t\text{BuOH} \quad (2)$$

$$R_3: \ \beta CHO + t\text{BuOOH} \rightarrow \text{HAP} \quad (3)$$

$$R_4: \ 3\ t\text{BuOOH} \underset{\text{CPO}}{\rightarrow} t\text{BuOH} + 2\ t\text{BuOO}^{\cdot} \quad (4)$$

$$R_5: \ \text{DHA} + t\text{BuOOH} \underset{\text{CPO}}{\rightarrow} {}_{ox}\text{DHA} + t\text{BuOH} \quad (5)$$

$$R_6: \ \text{DHA} + \beta CHO \underset{\text{FSA}}{\rightarrow} \text{preFagomine} \quad (6)$$

$$R_7: \ \text{preFagomine} \underset{\text{FSA}}{\rightarrow} \text{DHA} + \beta CHO \quad (7)$$

$$\frac{d[\beta OH]}{dt} = -r_1 \quad (8)$$

$$\frac{d[\beta CHO]}{dt} = r_1 - r_2 - r_3 - r_6 + r_7 \quad (9)$$

$$\frac{d[\beta COOH]}{dt} = r_2 \quad (10)$$

$$\frac{d[\text{HAP}]}{dt} = r_3 \quad (11)$$

$$\frac{d[t\text{BuOOH}]}{dt} = -r_1 - r_2 - r_3 - 3\ r_4 - r_5 \quad (12)$$

$$\frac{d[t\text{BuOH}]}{dt} = r_1 + r_2 + r_4 + r_5 \quad (13)$$

$$\frac{d[t\text{BuOO}^{\cdot}]}{dt} = 2\ r_4 \quad (14)$$

$$\frac{d[\text{DHA}]}{dt} = -r_5 - r_6 + r_7 \quad (15)$$

$$\frac{d[{}_{ox}\text{DHA}]}{dt} = r_5 \quad (16)$$

$$\frac{d[\text{preFagomine}]}{dt} = r_6 - r_7 \quad (17)$$

$$\frac{d(\text{CPOactivity})}{dt} = -kd_{CPO} \times \text{CPOactivity} \quad (18)$$

$$\frac{d(\text{FSAactivity})}{dt} = -(kd_{FSA1} + kd_{FSA2}) \times \text{FSAactivity} \quad (19)$$

All reactions were carried out in 1 ml of 0.1 M MES buffer (pH 6.5) at 25 °C, and stirred at 1000 rpm. The total withdrawn sampling volume was always kept below 10%. The concentrations of substrates and enzymes are specified in the corresponding text, figures and tables in SI section 3.

The estimation of model parameters was performed by progress curve analysis using PSE gPROMS® Model Builder 5.0.0, which allows the simultaneous determination of multiple parameters from several experiments. The optimization algorithm of the software was used to maximize the formation of preFagomine in simulated CPO/FSA reactions. Parameter Estimation in gPROMS was based on the Maximum Likelihood formulation which provides simultaneous estimation of parameters in both the physical model of the process and the variance model. MicroMath® Scientist® 2.0 was exclusively used for initial reaction rate analysis. Non-linear simplex and least squares fit regression methods implemented in SCIENTIST software were used for parameter estimation and model simulations. The software gives statistical output for the estimation of parameters, as well as goodness-of-fit statistics for the mathematical models.

2.7. Process intensification

All reactions were carried out in 0.1 M MES buffer (pH 6.5) at 25 °C, 1000 rpm with withdrawn volume below 10%, as follows: (a) The one-pot reaction was carried out in 1 ml at the following initial concentrations: 16 mM β-OH, 39.9 mM *t*-BuOOH, 72.6 mM DHA, 5.0 kU CPO ml^{-1} and 0.2 kU FSA ml^{-1}. (b) The initial two-step reaction mixture was 1 ml of 5.0 mM β-OH, 10.0 mM *t*-BuOOH, and 312.5 U CPO ml^{-1} for the β-OH oxidation, and 2 ml of 0.5 mM β-CHO, 20.0 mM DHA, and 0.58 U FSA ml^{-1} for the aldol addition. After the oxidation, the reaction medium was separated by a magnetic field (mNC) or filtration (agarose), and ultrafiltration (soluble enzyme, all cases). Finally, it was left under mild agitation for 60 min before starting the second reaction, to degrade all the peroxy radicals.

3. Results

A preliminary coupling of the CPO-catalyzed β-OH oxidation and the FSA-catalyzed DHA addition using soluble enzymes was investigated to choose the proper peroxide and buffer for the coupled reaction (SI section 2). Apart from the well-known inactivation of CPO caused by the peroxide, the reaction between β-CHO and the peroxide, and the oxidation of β-CHO to the acid, the main insight from this pre-analysis was: (a) *t*-BuOOH led to a notably higher alcohol oxidation rate than hydrogen peroxide. (b) The selected buffer was 100 mM MES buffer (pH 6.5) with high operational stability of both enzymes. (c) FSA was inactivated by incubation with CPO and *t*-BuOOH. (d) No preFagomine was obtained in a proof-of-concept reaction, probably due to a fast inactivation of FSA. (e) Various side reactions were identified on the complex system: the oxidation of DHA in presence of *t*-BuOOH and CPO –which competes with FSA for the use of DHA–, and the degradation of *t*-BuOOH catalyzed by CPO.

Fig. 2 includes the five side reactions and the inactivation of both enzymes within the whole reaction. All these undesirable phenomena hindered the simultaneous coupling of these two reactions. To overcome this issue, the development of a mathematical kinetic model was proposed as the work strategy. In contrast to a factorial design, a kinetic model might be able to relate the direct dependencies and effects of each reaction. To that end, all reaction and inactivation rates were intended to be individually investigated to reduce the disturbing effects of the other reactions, such as substrate or product inhibitions.

A separate kinetic model for each enzyme reaction was built. The model for CPO-catalyzed reactions was investigated by a stepwise method: (1) Incubation of CPO and *t*-BuOOH to determine the inactivation of CPO (kd_{CPO}). Here, $\mathbf{R_4}$ was also present. (2) Incubation of *t*-BuOOH and β-CHO to evaluate the chemical reaction ($\mathbf{R_3}$) that rendered the hydroxy alkyl peroxide (HAP). (3) Addition of β-CHO to step **1** for the interpretation of the oxidation of β-CHO to β-COOH. kd_{CPO}, $\mathbf{r_4}$ and $\mathbf{r_3}$ were also considered. (4) Addition of β-OH to previous steps to investigate the alcohol oxidation. Regarding the model for FSA-catalyzed reactions, it included two equilibrium reactions: $\mathbf{R_6}$ and $\mathbf{R_7}$. After its elucidation, both CPO/FSA systems were put together to study the oxidation of DHA by CPO and *t*-BuOOH, and the inactivation of FSA (kd_{FSA}) caused by the products from $\mathbf{R_4}$ and $\mathbf{R_5}$.

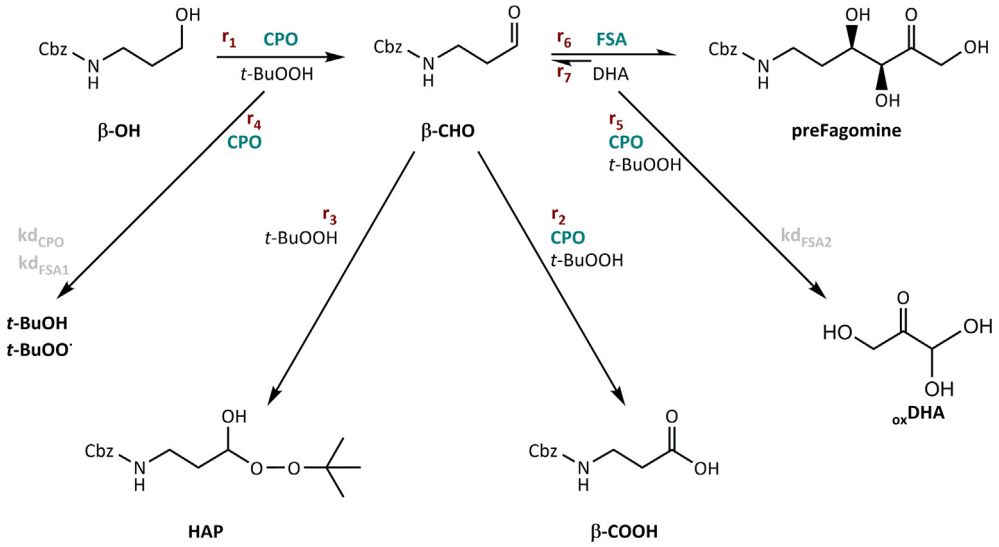

Fig. 2. Overall reaction mechanism including the identified side-reactions and the inactivation pathways for both enzymes.

3.1. CPO model

3.1.1. Degradation of t-BuOOH and CPO inactivation

$\mathbf{r_4}$ (mM min^{-1}) and kd_{CPO} (min^{-1}) were determined by the incubation of *t*-BuOOH and CPO (experimental distribution in Figure S5). A study of the initial reaction rates was discarded due to the peroxide-dependent fast inactivation of CPO. Instead, a progress curve analysis of each reaction was performed in terms of peroxide concentration and CPO activity over the reaction time. A sigmoidal behavior was observed for $\mathbf{r_4}$:

$$r_4 = \frac{k_{cat4} \times Y_{CPO} \times e^{-kd_{CPO}t} \times [t\text{BuOOH}]^n}{k_4^{\,n} + [t\text{BuOOH}]^n} \quad (20)$$

where Y_{CPO} corresponds to the CPO mass concentration (mg ml^{-1}), k_{cat4} is the turnover number in $\mathbf{R_4}$ (μmol min^{-1} mg^{-1}), whereas the inactivation of CPO (kd_{CPO}) was expressed as a function of $\mathbf{r_4}$; i.e. kd_{CPO} is proportional to the formation rate of the peroxyl radical *t*-BuOO· ($\mathbf{r_4}$) (Chamulitrat et al., 1989; Park and Clark, 2006):

$$kd_{CPO} = \frac{k_a \times r_4}{a + r_4} \quad (21)$$

where k_a is the maximum value of the CPO inactivation rate constant (min^{-1}), and a is an inactivation parameter (mM min^{-1}). This radical was assumed to be degraded in seconds, considering its accumulation in the reactor as negligible. The estimated values of all parameters are indicated in Table 1; Fig. 3 (3b in this case) shows some examples of the fitting to all the equations in the text (for all fittings, see Figure S6).

Regarding inhibitions affecting $\mathbf{r_4}$ or modulations over kd_{CPO}, it was not checked with β-OH, β-CHO or DHA at this step, as they are substrates of the same enzyme and consequently another reaction ($\mathbf{R_1}$, $\mathbf{R_2}$, $\mathbf{R_5}$) could interfere with the result. Inhibition/modulation was indeed evaluated with various concentrations of β-COOH and preFagomine, but no effect was observed (Figure S7).

3.1.2. Chemical reaction aldehyde–peroxide

To describe the rate of the chemical aldehyde–peroxide reaction ($\mathbf{r_3}$, mM min^{-1}), various concentrations of both compounds were mixed and left for incubation (Figure S8). Each reaction was analyzed in terms of concentrations of β-CHO and *t*-BuOOH over time (Fig. 3C, S9). Results indicated a classic equilibrium behavior from a reversible reaction:

$$r_3 = k_{3i} \times [\beta CHO] \times [t\text{BuOOH}] - k_{3ii} \times [\text{HAP}] \quad (22)$$

where k_{3i} is the forward chemical reaction constant (mM^{-1} min^{-1}), k_{3ii} is the reverse reaction constant (min^{-1}). β-OH, β-COOH, *t*-BuOH,

Table 1
Estimated values of the parameters in Equations (20)–(37). 95% confidence intervals are indicated.

Parameter	Value			Units
t-BuOOH degradation, CPO inactivation				
k_{cat4}	2.07	±	0.10	μmol · min^{-1} · mgCPO^{-1}
k_4	51.54	±	3.40	mM
n	1.43	±	0.02	–
k_a	$7.04 \cdot 10^{-2}$	±	$0.17 \cdot 10^{-2}$	min^{-1}
a	$1.83 \cdot 10^{-2}$	±	$0.20 \cdot 10^{-2}$	mM · min^{-1}
chemical reaction aldehyde–peroxide				
k_{3i}	$1.49 \cdot 10^{-3}$	±	$4 \cdot 10^{-5}$	mM^{-1} min^{-1}
k_{3ii}	$1.25 \cdot 10^{-1}$	±	$5 \cdot 10^{-3}$	min^{-1}
ki_{r3}	$2.18 \cdot 10^{-1}$	±	$1.4 \cdot 10^{-2}$	–
CPO-catalyzed reactions				
k_{cat2}	3.42	±	0.29	μmol · min^{-1} · mgCPO^{-1}
$K_{M,t\text{-BuOOH}}$	58.83	±	5.18	mM
$K_{M,\beta\text{-CHO}}$	36.38	±	3.84	mM
ki_{r4a}	6.52	±	0.04	mM
k_{cat1}	10.88	±	0.37	μmol · min^{-1} · mgCPO^{-1}
$K_{M,\beta\text{-OH}}$	309.5	±	12.0	mM
k_{cat5}	54.18	±	4.11	μmol · min^{-1} · mgCPO^{-1}
$K_{M,DHA}$	833.6	±	71.2	mM
ki_{r4b}	11.26	±	0.64	mM
ki_{r1}	108.2	±	8.5	mM
ki_{r2}	38.21	±	8.08	mM
ki_{r5}	32.15	±	0.76	mM
FSA-catalyzed reactions				
k_{cat6}	19.31	±	1.00	μmol · min^{-1} · mgFSA^{-1}
k_{cat7}	13.06	±	0.69	μmol · min^{-1} · mgFSA^{-1}
$K'_{M,DHA}$	9.00	±	1.70	mM
$K'_{M,\beta\text{-CHO}}$	20.94	±	2.25	mM
$K_{M,preFagomine}$	59.68	±	1.93	mM
ki_{r7}	$3.09 \cdot 10^{-1}$	±	$5.4 \cdot 10^{-2}$	mM
FSA inactivation				
k_1	$1.96 \cdot 10^{-1}$	±	$7 \cdot 10^{-3}$	mM^{-1}
k_2	6.70	±	0.24	mM^{-1}
k'_2	33.75	±	4.20	min^{-1}
b	3.45	±	0.41	mM · min^{-1}
c	$3.85 \cdot 10^{-1}$	±	$7 \cdot 10^{-3}$	–
d	$3.85 \cdot 10^{-2}$	±	$1.42 \cdot 10^{-2}$	–

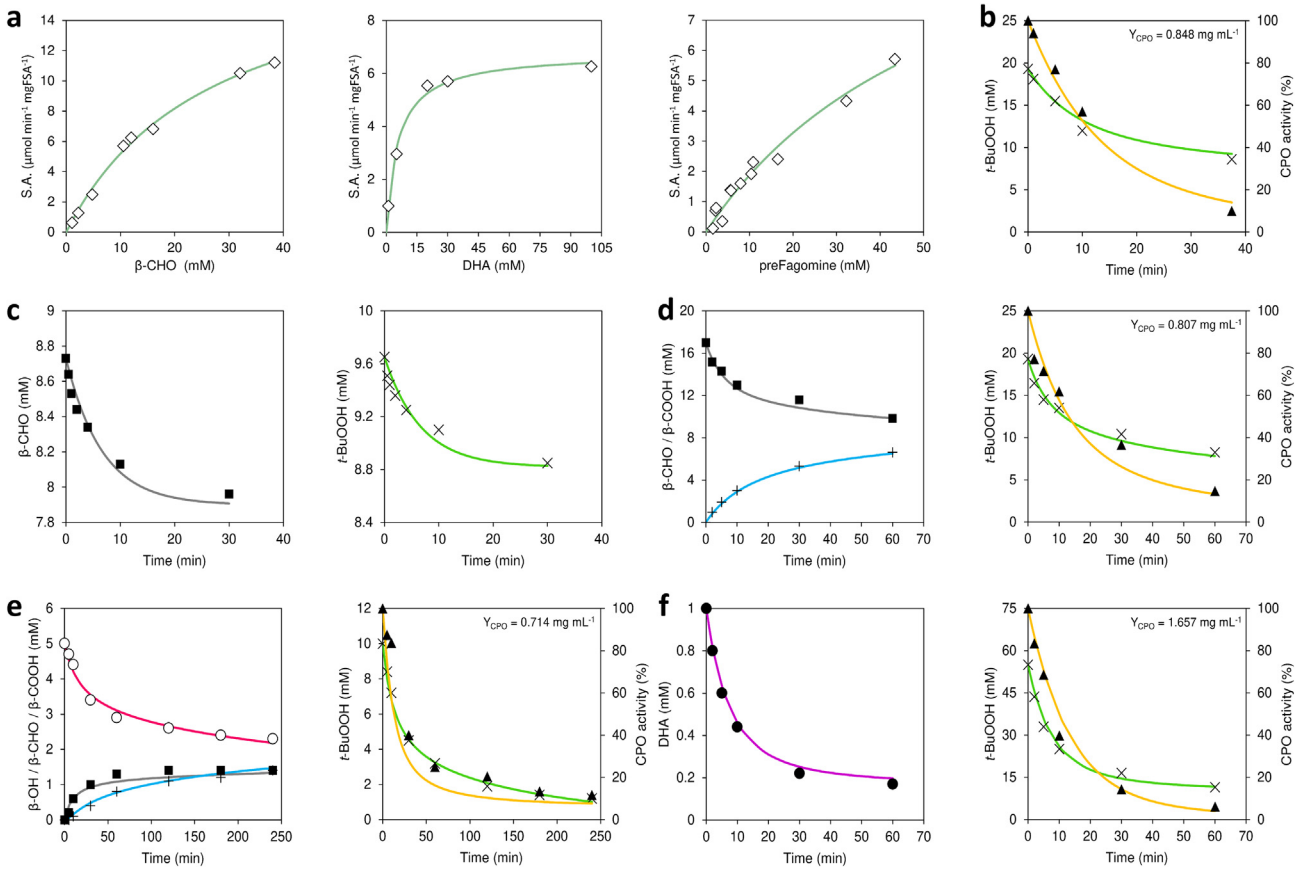

Fig. 3. Stepwise methodology for the kinetic model in the CPO/FSA reaction system. FSA-catalyzed reactions: (**a**) Initial reaction rates on $\mathbf{R_6}$ and $\mathbf{R_7}$; CPO-catalyzed reactions: (**b**) $\mathbf{R_4}$ and CPO inactivation caused by *t*-BuOO˙, (**c**) $\mathbf{R_3}$, (**d**) $\mathbf{R_2}$, $\mathbf{R_3}$, $\mathbf{R_4}$ and CPO inactivation, (**e**) $\mathbf{R_1}$, $\mathbf{R_2}$, $\mathbf{R_3}$, $\mathbf{R_4}$ and CPO inactivation, (**f**) $\mathbf{R_4}$, $\mathbf{R_5}$ and CPO inactivation. Experimental data: β-OH (○), β-CHO (■), β-COOH (+), *t*-BuOOH (×), DHA (●), CPO activity (▲); model: β-OH (▰), β-CHO (▰), β-COOH (▰), DHA (▰), *t*-BuOOH (▰), CPO activity (▰).

DHA, preFagomine were tested as inhibitors for this reaction. Only inhibition caused by β-COOH was observed (Figure S10), rewriting Eq. (22) with an extra inhibition term (ki_{r3}) (Figure S11):

$$r_3 = k_{3i} \times [\beta CHO] \times [t\text{BuOOH}] \times (1 + [\beta COOH])^{-ki_{r3}} - k_{3ii} \times [\text{HAP}] \quad (23)$$

3.1.3. CPO-catalyzed oxidations

Many reported reactions catalyzed by CPO exhibit an undeniable ping-pong mechanism (Casella et al., 1994; Colonna et al., 1999; Dunford, 2010; Kedderis and Hollenberg, 1983). The estimation of the kinetic parameters in these systems can be hindered by the tight relation between them. To overcome this limitation, a preliminary study of initial reaction rates was carried out to find an initial value of each parameter to be used for model calculations, according to:

$$r_1 = \frac{k_{cat1} \times Y_{CPO} \times e^{-kd_{CPO}t} \times [\beta OH] \times [t\text{BuOOH}]}{K_{M,\beta OH} \times [t\text{BuOOH}] + K_{M,t\text{BuOOH}} \times [\beta OH] + [t\text{BuOOH}] \times [\beta OH]} \quad (24)$$

$$r_2 = \frac{k_{cat2} \times Y_{CPO} \times e^{-kd_{CPO}t} \times [\beta CHO] \times [t\text{BuOOH}]}{K_{M,\beta CHO} \times [t\text{BuOOH}] + K_{M,t\text{BuOOH}} \times [\beta CHO] + [t\text{BuOOH}] \times [\beta CHO]} \quad (25)$$

$$r_5 = \frac{k_{cat5} \times Y_{CPO} \times e^{-kd_{CPO}t} \times [\text{DHA}] \times [t\text{BuOOH}]}{K_{M,\text{DHA}} \times [t\text{BuOOH}] + K_{M,t\text{BuOOH}} \times [\text{DHA}] + [t\text{BuOOH}] \times [\text{DHA}]} \quad (26)$$

where $K_{M,X}$ is the Michaelis constant of compound X. The initial reactions rates $\mathbf{r_1}$, $\mathbf{r_2}$ and $\mathbf{r_5}$ were analyzed together with $K_{M,t\text{-}BuOOH}$ as a global parameter (Figure S12, Table S2).

Regarding the CPO-oxidation of β-CHO into β-COOH, four reactions were studied in a mixture of CPO, β-CHO, *t*-BuOOH: degradation of the peroxide ($\mathbf{r_4}$), inactivation of CPO (kd_{CPO}), the chemical reaction ($\mathbf{r_3}$), and β-CHO oxidation ($\mathbf{r_2}$) (Eqs. (20), (21), (23), (25)). Several reactions with different concentrations of aldehyde and peroxide (Figure S13) were carried out to determine the actual value of the pre-estimated $\mathbf{r_2}$ parameters (Fig. 3D, S14). An inhibition mechanism in $\mathbf{r_4}$ caused by the amino aldehyde was observed from the experimental data, adding a new term (ki_{r4a}) to Eq. (20):

$$r_4 = \frac{k_{cat4} \times Y_{CPO} \times e^{-kd_{CPO}t} \times [\text{BuOOH}]^n}{k_4^{\,n} \times (1 + \frac{[\beta CHO]}{ki_{r4a}}) + [\text{BuOOH}]^n} \quad (27)$$

The best fitting results were obtained considering a competitive inhibition of β-CHO to the binding of the peroxide at the active site. The inhibition from other compounds of the reaction system, such as β-COOH, *t*-BuOH, and preFagomine on $\mathbf{r_2}$ was evaluated, but no inhibition was observed in any case (Figure S15).

To investigate the CPO-catalyzed oxidation of β-OH into β-CHO, several reactions with different concentrations of *t*-BuOOH and β-OH were carried out (Figure S16). Apart from $\mathbf{r_1}$ (Eq. (24)), other rates were considered: $\mathbf{r_2}$, $\mathbf{r_3}$, $\mathbf{r_4}$, and kd_{CPO} (Fig. 3E, S17). Regarding inhibitions affecting $\mathbf{r_1}$, it was not evaluated with β-COOH and preFagomine, since no inhibitory effect was observed for $\mathbf{r_2}$.

Reactions with different peroxide and DHA concentrations were carried out (Figure S18) to estimate the kinetic parameters from Eq. (26). $\mathbf{r_4}$ and CPO inactivation should be also considered apart

from $\mathbf{r_5}$ (Fig. 3F, S19). An inhibition mechanism in $\mathbf{r_4}$ caused by DHA was observed from the experimental data, adding an inhibition term ki_{r4b}:

$$r_4 = \frac{k_{cat4} \times Y_{CPO} \times e^{-kd_{CPO}t} \times [t\text{BuOOH}]^n}{k_4{}^n \times (1 + \frac{[\beta CHO]}{ki_{r4a}} + \frac{[DHA]}{ki_{r4b}}) + [t\text{BuOOH}]^n} \quad (28)$$

The best results were obtained considering a competitive inhibition of DHA to the binding of the peroxide at the active site.

To check for possible interactions of $\mathbf{r_5}$ with $\mathbf{r_1}$ or $\mathbf{r_2}$, five reactions were performed with a fixed concentration of CPO, β-OH, and *t*-BuOOH, but a variable amount of DHA (Figures S20). Three inhibition terms were added: two competitive inhibitions of DHA to the binding of β-OH or β-CHO to the active site (ki_{r1}, ki_{r2}), and the competitive inhibition of β-OH to the binding of DHA (ki_{r5}):

$$r_1 = \frac{k_{cat1} \times Y_{CPO} \times e^{-kd_{CPO}t} \times [\beta OH] \times [t\text{BuOOH}]}{K_{M,\beta OH} \times (1 + \frac{[DHA]}{ki_{r1}}) \times [t\text{BuOOH}] + K_{M,t\text{BuOOH}} \times [\beta OH] + [t\text{BuOOH}] \times [\beta OH]} \quad (29)$$

$$r_2 = \frac{k_{cat2} \times Y_{CPO} \times e^{-kd_{CPO}t} \times [\beta CHO] \times [t\text{BuOOH}]}{K_{M,\beta CHO} \times (1 + \frac{[DHA]}{ki_{r2}}) \times [t\text{BuOOH}] + K_{M,t\text{BuOOH}} \times [\beta CHO] + [t\text{BuOOH}] \times [\beta CHO]} \quad (30)$$

$$r_5 = \frac{k_{cat5} \times Y_{CPO} \times e^{-kd_{CPO}t} \times [DHA] \times [t\text{BuOOH}]}{K_{M,DHA} \times (1 + \frac{[\beta OH]}{ki_{r5}}) \times [t\text{BuOOH}] + K_{M,t\text{BuOOH}} \times [DHA] + [t\text{BuOOH}] \times [DHA]} \quad (31)$$

3.2. FSA model

FSA is a class I aldolase and, therefore, the conserved active lysine in the enzyme active site forms a Schiff base intermediate with DHA (substrate A), which attacks the carbonyl carbon of substrate B (β-CHO) (Schürmann and Sprenger, 2001). The aldol and retroaldol additions ($\mathbf{r_6}$, $\mathbf{r_7}$) are then described as an ordered sequential mechanism:

$$r_6 = \frac{k_{cat6} \times Y_{FSA} \times [DHA] \times [\beta CHO]}{K'_{M,\beta CHO} \times [DHA] + K'_{M,DHA} \times K'_{M,\beta CHO} + [DHA] \times [\beta CHO]} \quad (32)$$

$$r_7 = \frac{k_{cat7} \times Y_{FSA} \times [\text{preFagomine}]}{K_{M,\text{preFagomine}} + [\text{preFagomine}]} \quad (33)$$

Contrarily to CPO, no inactivation of FSA was expected among its reactions; an initial reaction rate analysis can be easily performed to estimate the parameters. To this end, several reactions were performed varying the concentration of DHA or β-CHO, and preFagomine, analyzing the reaction rate before 10% of substrate conversion was achieved (Fig. 3a).

To check if there is any inhibition between both reactions, various reactions with different concentrations of β-CHO and DHA were carried out (Figure S21). As it has been already reported elsewhere (Sudar et al., 2013a), product inhibition by the amino aldehyde was observed in the retroaldol addition, adding an inhibition term (Figure S22):

$$r_7 = \frac{k_{cat7} \times Y_{FSA} \times [\text{preFagomine}]}{K_{M,\text{preFagomine}} \times (1 + \frac{[\beta CHO]}{ki_{r7}}) + [\text{preFagomine}]} \quad (34)$$

3.2.1. Coupled system: FSA inactivation

The inactivation of FSA in the whole CPO/FSA system was characterized for the eventual use of this model for the coupled reaction, distinguishing two inactivation pathways: kd_{FSA1} and kd_{FSA2}. Regarding kd_{FSA1}, FSA was incubated with different concentrations of *t*-BuOOH and CPO (Figure S23). The inactivation was mathematically expressed as a linear dependence of $\mathbf{r_4}$ (Figure S24):

$$kd_{FSA1} = k_1 \times r_4 \quad (35)$$

Regarding the second inactivation (kd_{FSA2}), incubations of FSA and CPO with different concentrations of *t*-BuOOH and DHA (Figure S25) were carried out. Again, the inactivation was described with a linear expression, not related to $\mathbf{r_4}$ but to the oxidation of DHA by CPO ($\mathbf{r_5}$) (Figure S26).

$$kd_{FSA2} = k_2 \times r_5 \quad (36)$$

Additional series of experiments were performed to confirm the obtained kinetic values for the inactivation of FSA, mixing different concentrations of β-OH, DHA, *t*-BuOOH, CPO and FSA (Table S3). The fittings from these experiments (Figure S27) indicated: (1) kd_{FSA1} was confirmed to be a linear function of r_4, (2) kd_{FSA2} was not a linear function of $\mathbf{r_5}$, but a hyperbolic function as already described for FSA reactions (Česnik et al., 2019), (3) an increase of Y_{FSA} acts as a positive modulator effect on FSA activity, lowering kd_{FSA2}; (4) (an increase of the DHA concentration leads a higher $\mathbf{r_5}$, which produces a more rapid inactivation of FSA. However, DHA is a natural substrate of FSA and may protect the active site of FSA from inactivation:

$$kd_{FSA2} = \frac{k'_2 \times r_5}{b + r_5} \times (1 + Y_{FSA})^{-c} \times (1 + [DHA])^{-d} \quad (37)$$

3.3. Model validation

For the validation of all estimated kinetic parameters, several reactions were carried out fixing the concentration of β-OH, *t*-BuOOH and CPO at high values (47.0 mM, 77.7 mM, 0.714 mg mL^{-1}) to increase the productivity of preFagomine. Since the concentrations of DHA and FSA are the most sensitive variables to the inactivation of FSA, up to seven reactions were carried out with different concentrations of these two variables (Figure S28). The model fitted all the data correctly (Fig. 4, Figure S29), although very low concentrations of preFagomine were obtained at each of these conditions. This could be overcome by model exploitation, optimizing the reaction conditions to increase the product yield. Besides, the use of immobilized enzymes could enhance the compatibility between both enzymes, lowering their inactivation rates.

3.4. Model exploitation for process intensification

3.4.1. One-pot strategy

The constructed mathematical model was used to find the optimal conditions for the one-pot approach reaction. The variables for optimization were the initial concentrations of all substrates (*t*-BuOOH, β-OH, DHA) and enzymes (CPO and FSA) (Table S4). The optimal initial Y_{CPO} and Y_{FSA} were predicted at the upper bound of the variable range used in the optimization (Table S5); this range was not further increased due to medium viscosity. Considering a reaction time of 5 h, the model predicts that a high quantity of both enzymes is required to obtain a moderate preFagomine yield of 14.6%. The predicted values were experimentally confirmed by a coupled reaction at these initial conditions using both soluble CPO and FSA, double-checking the applicability of the model and the unfeasibility of the coupled system. Some accumulation of the aldehyde was observed at the end of the reaction due to the high instability of FSA (CPO remained active at 66%). No immobilized derivatives were tested in the one-pot configuration due to a required enzyme load too high to be immobilized on the support (considering 5% v/v support/reaction-medium for pseudo-homogeneous catalysis).

A (semi)continuous addition of peroxide, DHA and/or enzymes was considered as a strategy to overcome the inactivation of FSA. Preliminary simulations, however, indicated lower oxidation and

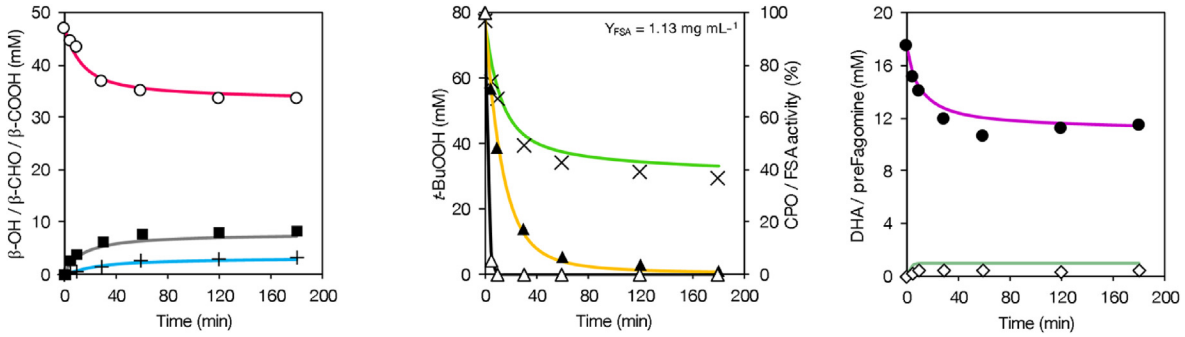

Fig. 4. Fitting example of one of the reactions used in the CPO/FSA model validation. Experimental data: β-OH (○), β-CHO (■), β-COOH (+), DHA (●), *t*-BuOOH (×), preFagomine (◇), CPO activity (▲), FSA activity (△); model simulation: β-OH (▬), β-CHO (▬), β-COOH (▬), DHA (▬), *t*-BuOOH (▬), preFagomine (▬), CPO activity (▬), FSA activity (▬).

aldol addition rates, ruling out this strategy. An alternative operation to one-pot is the separation of both reactions, performing the overall reaction as two consecutive reaction cascade. That avoids the oxidation of DHA, the inhibition of CPO reactions by DHA, and the inactivation of FSA.

3.4.2. Two-step reaction

The two-step coupled reaction was carried out in two separate vessels with an intermediate step of ultrafiltration to remove CPO from the reaction medium. The filtered mixture was left under mild agitation for 60 min to ensure the degradation of the formed radical.

The optimal initial conditions were predicted by a different optimization procedure: to enable the further use of immobilized CPO and FSA in the reaction, the enzyme concentration was fixed at the maximum enzyme load maintaining the 5% v/v support/medium (SI section 3.13). Then the optimal values for the two variables in the oxidation reaction (initial concentration of β-OH and *t*-BuOOH) and one variable in the aldol addition reaction (initial concentration of DHA) were predicted.

First, the two-step reaction was carried out using both soluble CPO and FSA (Fig. 5a). Regarding the oxidation of β-OH, the model accurately predicted the experimental data, leading to a β-CHO yield of 17.9% (expected: 18.4%). The reaction was stopped after 5 h when the measured activity of CPO was negligible; the pseudo half-life time of the enzyme (CPO-$t_{1/2}$) was only 18 min. The reaction mixture was filtered, and the aldol addition was started after 60 min. Here, however, the kinetic model was not able to predict the experimental data: the measured preFagomine yield was 38.4%, whereas the predicted one was 79.3%. The latter value was

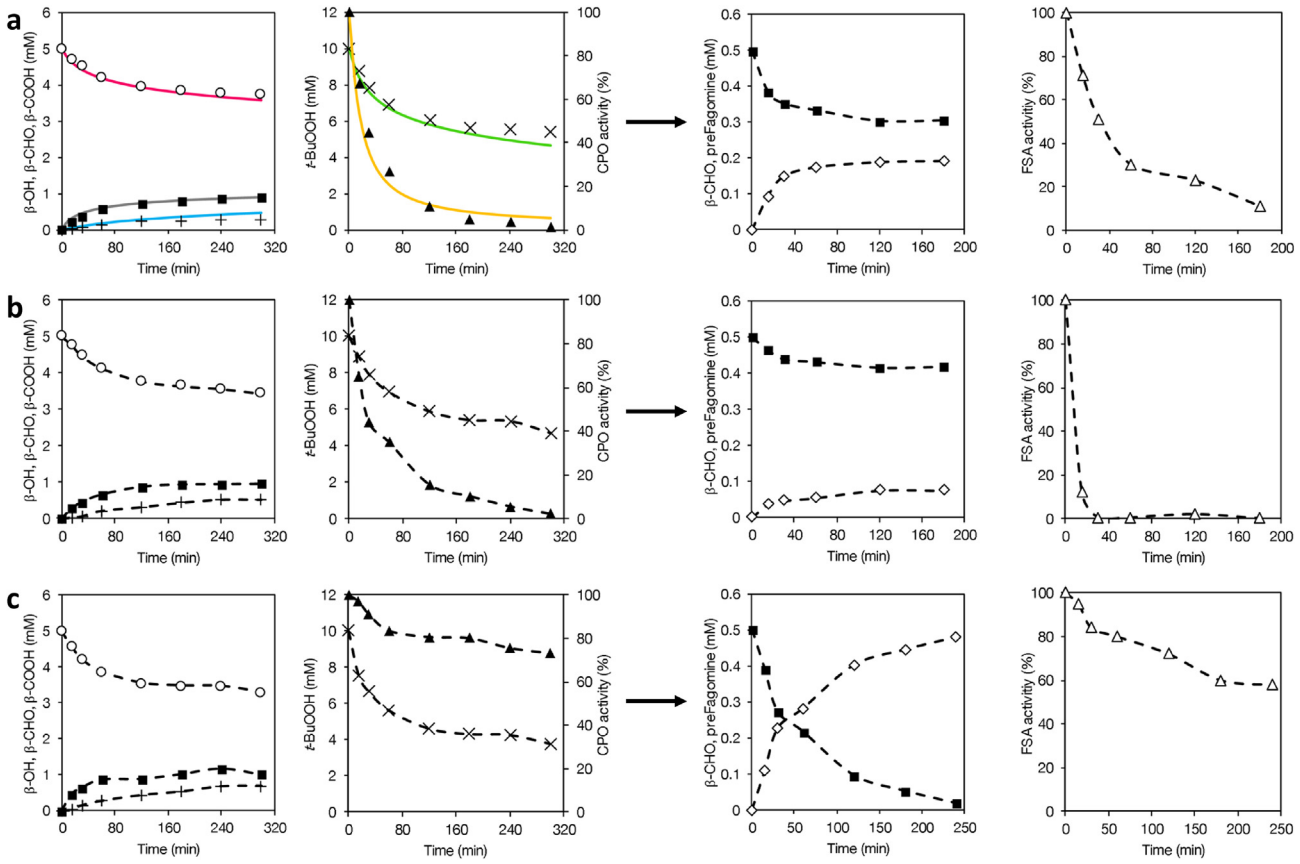

Fig. 5. CPO and FSA-catalyzed two-step synthesis of preFagomine. (**a**) Soluble enzymes, (**b**) mNC-enzymes, (**c**) agarose-enzymes. Experimental data: β-OH (○), β-CHO (■), β-COOH (+), *t*-BuOOH (×), preFagomine (◇), CPO activity (▲), FSA activity (△); model simulation: β-OH (▬), β-CHO (▬), β-COOH (▬), *t*-BuOOH (▬), CPO activity (▬).

confirmed by performing an aldol addition reaction using commercial β-CHO at the same reaction conditions (Figure S30) with a preFagomine yield of 81.1%. Therefore, the difference might be caused by the inactivation of FSA. Although no inactivation was expected, the soluble FSA activity dropped more than 80% in 3 h (FSA-$t_{1/2}$ = 35 min), probably because some inactivating agent was not removed from the mixture, and it inactivated the enzyme. Further stabilization was expected by using immobilized enzymes, either onto nanoparticles or conventional agarose supports.

Four derivatives ($_n$CPO-MANA-agarose, mNC-NH_2-CPO, FSA-CoIDA-agarose, mNC-NH_2-FSA) were tested at the optimized reaction conditions. However, it should be noted that when immobilized enzymes are used, the kinetic parameters can differ from the ones found for the soluble catalysts due to mass transfer effects or altered inactivation rates due to immobilization (Illanes, 2008).

The β-OH oxidation catalyzed by mNC-NH_2-CPO led to similar results than the soluble CPO (Fig. 5b). The amino aldehyde yield was 19.0% at the same reaction time (5 h), while no improvement in the operational stability of the enzyme was observed (CPO-$t_{1/2}$ = 24 min, 1.3-fold increase). In the aldol addition catalyzed by mNC-NH_2-FSA, a lower preFagomine yield (15.0%) was obtained, likely related to the rapid inactivation of FSA through this immobilization strategy (FSA-$t_{1/2}$ = 8 min). Regarding the agarose derivatives, the oxidation of CPO on MANA-agarose (Fig. 5c) gave similar results with a β-CHO yield of 20.2%. Although the enzyme remained active after 5 h (CPO-$t_{1/2} \gg$ 300 min, ≫17-fold increase), the reaction was stopped because the amino aldehyde concentration reached a *plateau*. FSA immobilized on CoIDA-agarose led to the best results in the aldol addition reaction, with a preFagomine yield of 96.3% (this reaction was left for 4 h since FSA remained active, FSA-$t_{1/2}$ ≫240 min, ≫7-fold increase). Although diffusional limitations in the activity test can hinder its interpretation, FSA stability is truly enhanced by the immobilization of the enzyme into CoIDA-agarose.

With the last catalytic complex formed by CPO-MANA-agarose/FSA-CoIDA, the highest final overall yield of the two-step reaction was obtained: 19.5%. In comparison to the one-pot reaction using soluble enzymes, the results are incredibly promising: (a) in the one-pot approach, only 1.82 μmol preFagomine were obtained from 16.0 μmol β-OH using 85 μmol CPO and 52 μmol FSA, with a total production of 0.026 $mmol_{preFagomine}$ $mol^{-1}_{\beta\text{-OH}}$ mol^{-1}_{CPO} mol^{-1}_{FSA}. (b) In the two-step reaction with agarose derivatives, 0.96 μmol preFagomine were obtained from 5.0 μmol β-OH using 12.8 μmol CPO and 0.31 μmol FSA (concentrations considering the activity loss during the immobilization procedure), with a total production of 47.8 $mmol_{preFagomine}$ $mol^{-1}_{\beta\text{-OH}}$ mol^{-1}_{CPO} mol^{-1}_{FSA}. That denotes an 1839-fold increase of the specific preFagomine production of the presented immobilized system on the coupled reaction.

4. Conclusions

The feasibility of a multi-enzymatic reaction cascade to synthesize iminocyclitols using amino alcohols as the starting material has been investigated. Particularly, the coupled CPO-catalyzed β-OH oxidation and FSA-catalyzed DHA aldol addition that renders preFagomine are investigated in detail. A mathematical model for better understanding of the reaction kinetics of the whole system was developed by an in-depth study of each individual reaction separately. This is crucial for avoiding undesired interactions among reactions which could hinder the analysis of the results. Up to 7 reactions were investigated, estimating their kinetic parameters: degradation of peroxide, chemical reaction, amino aldehyde oxidation, alcohol oxidation, DHA oxidation, aldol addition, and retroaldol addition. The inactivation of both enzymes was also described. The kinetic model was validated with great fitting of the experimental data, enabling the comprehension of this highly complex reaction system by identifying the inactivation of FSA as the main bottleneck. Our study elucidated the coupled reaction mechanisms, showing the inhibitions among diverse substrates and products from the different reactions.

The kinetic model was used for process intensification, determining the optimal conditions for the coupling in two reactor configurations: one-pot synthesis or two-consecutive vessels approach. Both strategies were investigated in detail using soluble and immobilized CPO/FSA. The separation of the oxidation and the aldol addition notably reduced the inactivation of FSA driven by CPO, led to a higher enzyme stability (17-fold increase for CPO, 7-fold for FSA), and incremented the product synthesis. The most promising results were obtained in the two-step reaction catalyzed by CPO-MANA-agarose and FSA-CoIDA-agarose, with an 1839-fold increase on the preFagomine production per mol of enzyme in comparison to the one-pot approach with soluble enzymes.

Declaration of Competing Interest

The authors declare that they have no known competing financial interests or personal relationships that could have appeared to influence the work reported in this paper.

Acknowledgments

This work was supported by Spanish MINECO (project No. CTQ2014-53114R), co-financed by European Regional Development Fund. The Department of Chemical, Biological and Environmental Engineering of UAB constitutes the Biochemical Engineering Unit of the Reference Network in Biotechnology, and the research group 2014SGR452, Generalitat de Catalunya. Financial support from Spanish MINECO for the PhD scholarship of Gerard Masdeu is acknowledged. The authors acknowledge the financial support from the Slovenian Research Agency (ARRS) for Research Core Funding (P2-0089) and ARRS Project (J1-7302), and the financial support for the research work in the host institutions (Jožef Stefan Institute, University of Zagreb) from the European Comission (Erasmus program) and COST-STSM-CM1303.

The authors thank Dr. Alba Eustaquio and Dr. Maria Jesús Ibarz from Servei d'Anàlisi Química of the Universitat Autònoma de Barcelona for their assistance on mass spectrometry analyses.

Appendix A. Supplementary material

Supplementary data to this article can be found online at https://doi.org/10.1016/j.ces.2021.116602.

References

Andersson, L., Wolfenden, R., 1982. A General Method of aplha-Aminoaldehyde Synthesis Using Alcohol Dehydrogenase. Anal. Biochem. 124, 150–157. https://doi.org/10.1016/0003-2697(82)90232-9.

Andersson, M., Andersson, M.M., Adlercreutz, P., 2000. Stabilisation of Chloroperoxidase Towards Peroxide Dependent Inactivation. Biocatal. Biotransformat. 18, 457–469. https://doi.org/10.3109/10242420009015263.

Ardao, I., Benaiges, M.D., Caminal, G., Álvaro, G., 2006. One step purification-immobilization of fuculose-1-phosphate aldolase, a class II DHAP dependent aldolase, by using metal-chelate supports. Enzyme Microb. Technol. 39, 22–27. https://doi.org/10.1016/j.enzmictec.2005.09.001.

Ayala, M., Batista, C.V., Vazquez-Duhalt, R., 2011. Heme destruction, the main molecular event during the peroxide-mediated inactivation of chloroperoxidase from Caldariomyces fumago. J. Biol. Inorg. Chem. 16, 63–68. https://doi.org/10.1007/s00775-010-0702-6.

Banba, Y., Abe, C., Nemoto, H., Kato, A., Adachi, I., Takahata, H., 2001. Asymmetric synthesis of fagomine and its congeners. Tetrahedron Asymmetry 12, 817–819. https://doi.org/10.1016/S0957-4166(01)00136-7.

Calleja, D., Kavanagh, J., de Mas, C., López-Santín, J., 2016. Simulation and prediction of protein production in fed-batch E. coli cultures: An engineering approach. Biotechnol. Bioeng. 113, 772–782. https://doi.org/10.1002/bit.25842.

Calveras, J., Egido-Gabás, M., Gómez, L., Casas, J., Parella, T., Joglar, J., Bujons, J., Clapés, P., 2009. Dihydroxyacetone phosphate aldolase catalyzed synthesis of structurally diverse polyhydroxylated pyrrolidine derivatives and evaluation of their glycosidase inhibitory properties. Chem. - A Eur. J. 15, 7310–7328. https://doi.org/10.1002/chem.200900838.

Casella, L., Poli, S., Gullotti, M., Selvaggini, C., Beringhelli, T., Marchesini, A., 1994. The chloroperoxidase-catalyzed oxidation of phenols. Mechanism, selectivity, and characterization of enzyme-substrate complexes. Biochemistry 33, 6377–6386. https://doi.org/10.1021/bi00187a001.

Castillo, J.A., Calveras, J., Casas, J., Mitjans, M., Vinardell, M.P., Parella, T., Inoue, T., Sprenger, G. a., Joglar, J., Clapés, P., 2006. Fructose-6-phosphate aldolase in organic synthesis: Preparation of D-fagomine, N-alkylated derivatives, and preliminary biological assays. Org. Lett. 8, 6067–6070. https://doi.org/10.1021/ol0625482

Castillo, J.A., Guérard-Hélaine, C., Gutiérrez, M., Garrabou, X., Sancelme, M., Schürmann, M., Inoue, T., Hélaine, V., Charmantray, F., Gefflaut, T., Hecquet, L., Joglar, J., Clapés, P., Sprenger, G.A., Lemaire, M., 2010. A mutant D-fructose-6-phosphate aldolase (Ala129Ser) with improved affinity towards dihydroxyacetone for the synthesis of polyhydroxylated compounds. Adv. Synth. Catal. 352, 1039–1046. https://doi.org/10.1002/adsc.200900772.

Česnik, M., Sudar, M., Roldan, R., Hernandez, K., Parella, T., Clapés, P., Charnock, S., Vasić-Rački, Đ., Findrik Blažević, Z., 2019. Model-based optimization of the enzymatic aldol addition of propanal to formaldehyde: A first step towards enzymatic synthesis of 3-hydroxybutyric acid. Chem. Eng. Res. Des. 150, 140–152. https://doi.org/10.1016/j.cherd.2019.06.025.

Chamulitrat, W., Takahashi, N., Mason, R.P., 1989. Peroxyl, alkoxyl, and carbon-centered radical formation from organic hydroperoxides by chloroperoxidase. J. Biol. Chem. 264, 7889–7899. https://doi.org/10.1016/S0021-9258(18)83127-1.

Colonna, S., Gaggero, N., Richelmi, C., Pasta, P., 1999. Recent biotechnological developments in the use of peroxidases. Trends Biotechnol. 17, 163–168. https://doi.org/10.1016/S0167-7799(98)01288-8.

Dunford, H.B., 2010. Peroxidases and Catalases: Biochemistry, Biophysics, Biotechnology and Physiology. John Wiley & Sons, NJ, USA. https://doi.org/10.1002/cbic.200000397

Fan, J.Q., Ishii, S., Asano, N., Suzuki, Y., 1999. Accelerated transport and maturation of lysosomal alpha-galactosidase A in Fabry lymphoblasts by an enzyme inhibitor. Nat. Med. 5, 112–115. https://doi.org/10.1038/4801.

Ferioli, V., Vezzalini, E., Rustichelli, C., Gamberini, G., 1995. High-Performance Liquid Chromatography of Dihydroxyacetone as its bis-2,4-Dinitrophenylhydrazone Derivative. Chromatographia 41, 61–65. https://doi.org/10.1007/BF02688001.

Fernandez-Lafuente, R., Rosell, C.M., Rodriguez, V., Santana, C., Soler, G., Bastida, A., Guisan, J.M., 1993. Preparation of activated supports containing low pK amino groups. A new tool for protein immobilization via the carboxyl coupling method. Enzyme Microb. Technol. 15, 546–550. https://doi.org/10.1016/0141-0229(93)90016-u.

Fleet, G.W.J., Fellows, L.E., Smith, P.W., 1987. Synthesis of deoxymannojirimycin fagomine deoxynojirimycin 2-acetamido-1,5-imino-1,2,5-trideoxy-D-mannitol 2-acetamido-1,5-imino-1,2,5-trideoxy-D-glucitol 2S,3R,4R,5R-trihydroxypipecolic acid and 2S,3R,4R,5S-trihydroxypipecolic acid from methyl 3-O-benzyl. Tetrahedron 43, 979–990. https://doi.org/10.1016/S0040-4020(01)90035-3.

Gloster, T.M., Meloncelli, P., Stick, R.V., Zechel, D., Vasella, A., Davies, G.J., 2007. Glycosidase inhibition: An assessment of the binding of 18 putative transition-state mimics. J. Am. Chem. Soc. 129, 2345–2354. https://doi.org/10.1021/ja066961g.

Gómez, L., Molinar-Toribio, E., Calvo-Torras, M.Á., Adelantado, C., Juan, M.E., Planas, J.M., Cañas, X., Lozano, C., Pumarola, S., Clapés, P., Torres, J.L., 2012. d-Fagomine lowers postprandial blood glucose and modulates bacterial adhesion. Br. J. Nutr. 107, 1739–1746. https://doi.org/10.1017/S0007114511005009.

Goujon, J.Y., Gueyrard, D., Compain, P., Martin, O.R., Ikeda, K., Kato, A., Asano, N., 2005. General synthesis and biological evaluation of α-1-C-substituted derivatives of fagomine (2-deoxynojirimycin-α-C-glycosides). Bioorganic Med. Chem. 13, 2313–2324. https://doi.org/10.1016/j.bmc.2004.12.043.

Guisán, J., 1988. Aldehyde-agarose gels as activated supports for immobilization-stabilization of enzymes. Enzyme Microb. Technol. 10, 375–382. https://doi.org/10.1016/0141-0229(88)90018-X.

Gutierrez, M., Parella, T., Joglar, J., Bujons, J., Clapés, P., 2011. Structure-guided redesign of D-fructose-6-phosphate aldolase from E. coli: remarkable activity and selectivity towards acceptor substrates by two-point mutation. Chem. Commun. 47, 5762–5764. https://doi.org/10.1039/c1cc11069a.

Hereu, M., Ramos-Romero, S., Marín-Valls, R., Amézqueta, S., Miralles-Pérez, B., Romeu, M., Méndez, L., Medina, I., Torres, J.L., 2019. Combined buckwheat d-fagomine and fish omega-3 pufas stabilize the populations of gut prevotella and bacteroides while reducing weight gain in rats. Nutrients 11. https://doi.org/10.3390/nu11112606.

Herna, K., Bujons, J., Parella, T., Rolda, R., 2019. Aldolase-Catalyzed Asymmetric Synthesis of N-Heterocycles by Addition of Simple Aliphatic Nucleophiles to Aminoaldehydes. Adv. Synth. Catal. 361, 2673–2687. https://doi.org/10.1002/adsc.201801530.

Illanes, A., 2008. Enzyme biocatalysis: Principles and applications, Enzyme Biocatalysis: Principles and Applications. https://doi.org/10.1007/978-1-4020-8361-7

Kedderis, G.L., Hollenberg, P.F., 1983. Steady state kinetics of chloroperoxidase-catalyzed N-demethylation reactions. J. Biol. Chem. 258, 12413–12419. https://doi.org/10.1016/S0021-9258(17)44191-3.

Koyama, M., Sakamura, S., 1974. The Structure of a New Piperidine Derivative from Buckwheat Seeds (Fagopyrum esculentum Moench). Agric. Biol. Chem. 38, 1111–1112. https://doi.org/10.1080/00021369.1974.10861295.

Kralj, S., Drofenik, M., Makovec, D., 2011. Controlled surface functionalization of silica-coated magnetic nanoparticles with terminal amino and carboxyl groups. J. Nanoparticle Res. 13, 2829–2841. https://doi.org/10.1007/s11051-010-0171-4.

Kralj, S., Makovec, D., 2015. Magnetic Assembly of Superparamagnetic Iron Oxide Nanoparticle Clusters into Nanochains and Nanobundles. ACS Nano 9, 9700–9707. https://doi.org/10.1021/acsnano.5b02328.

Kralj, S., Makovec, D., Čampelj, S., Drofenik, M., 2010. Producing ultra-thin silica coatings on iron-oxide nanoparticles to improve their surface reactivity. J. Magn. Magn. Mater. 322, 1847–1853. https://doi.org/10.1016/j.jmmm.2009.12.038.

Kumari, N., Reddy, B.G., Vankar, Y.D., 2009. Efficient and stereodivergent syntheses of D- and L-fagomines and their analogues. European J. Org. Chem. 160–169. https://doi.org/10.1002/ejoc.200800796.

Lenoir, D., 2006. Selective oxidation of organic compounds-sustainable catalytic reactions with oxygen and without transition metals?. Angew. Chem. Int. Ed. 45, 3206–3210. https://doi.org/10.1002/anie.200502702.

Masdeu, G., Kralj, S., Pajk, S., López-Santín, J., Makovec, D., Álvaro, G., 2018. Hybrid chloroperoxidase-magnetic nanoparticle clusters: Effect of functionalization on biocatalyst performance. J. Chem. Technol. Biotechnol. 93, 233–245. https://doi.org/10.1002/jctb.5345.

Masdeu, G., Pérez-Trujillo, M., López-Santín, J., Álvaro, G., 2016a. Chloroperoxidase-catalyzed amino alcohol oxidation: Substrate specificity and novel strategy for the synthesis of N-Cbz-3-aminopropanal. Process Biochem. 51, 1204–1211. https://doi.org/10.1016/j.procbio.2016.05.022.

Masdeu, G., Pérez-Trujillo, M., López-Santín, J., Álvaro, G., 2016b. Data on the identification and characterization of by-products from N-Cbz-3-aminopropanal and t-BuOOH/H2O2 chemical reaction in chloroperoxidase-catalyzed oxidations. Data Br. 8, 659–665. https://doi.org/10.1016/j.dib.2016.06.028.

Masdeu, G., Vázquez, L.M., López-Santín, J., Caminal, G., Kralj, S., Makovec, D., Álvaro, G., Guillén, M., 2021. Synthesis of a precursor of D-fagomine by immobilized fructose-6-phosphate aldolase. PLoS One. https://doi.org/10.1371/journal.pone.0250513.

Morris, D.R., Hager, L.P., 1966. Chloroperoxidase I. Isolation and Properties of the crystalline Glycoprotein. J. Biol. Chem. 241, 1763–1768. https://doi.org/10.1016/S0021-9258(18)96701-3.

Nojima, H., Kimura, I., Chen, F.J., Sugihara, Y., Haruno, M., Kato, a, Asano, N., 1998. Antihyperglycemic effects of N-containing sugars from Xanthocercis zambesiaca, Morus bombycis, Aglaonema treubii, and Castanospermum australe in streptozotocin-diabetic mice. J. Nat. Prod. 61, 397–400. https://doi.org/10.1021/np970277l

Pandey, G., Kapur, M., 2000. A general strategy towards the synthesis of 1-N-iminosugar type glycosidase inhibitors: demonstration by the synthesis of d- as well as l-glucose type iminosugars (isofagomines). Tetrahedron Lett. 41, 8821–8824. https://doi.org/10.1016/S0040-4039(00)01553-7.

Park, J.-B., Clark, D.S., 2006. Deactivation Mechanisms of Chloroperoxidase During Biotransformations. Biotechnol. Bioeng. 93, 1190–1195. https://doi.org/10.1002/bit.

Pearson, M.S.M., Mathé-Allainmat, M., Fargeas, V., Lebreton, J., 2005. Recent advances in the total synthesis of piperidine azasugars. European J. Org. Chem. 2159–2191. https://doi.org/10.1002/ejoc.200400823.

Pešić, M., López, C., Álvaro, G., López-Santín, J., 2012. A novel immobilized chloroperoxidase biocatalyst with improved stability for the oxidation of amino alcohols to amino aldehydes. J. Mol. Catal. B Enzym. 84, 144–151. https://doi.org/10.1016/j.molcatb.2012.04.010.

Robertson, J.G., 2005. Mechanistic basis of enzyme-targeted drugs. Biochemistry 44, 5561–5571. https://doi.org/10.1021/bi050247e.

Rodriguez-Hinestroza, R.A., Lopez, C., Lopez-Santin, J., Kane, C., Dolors Benaiges, M., Tzedakis, T., 2017. HLADH-catalyzed synthesis of beta-amino acids, assisted by continuous electrochemical regeneration of NAD+ in a filter press microreactor. Chem. Eng. Sci. 158, 196–207. https://doi.org/10.1016/j.ces.2016.10.010.

Schürmann, M., Sprenger, G.A., 2001. Fructose-6-phosphate Aldolase is a Novel Class I Aldolase from Escherichia coli and is Related to a Novel Group of Bacterial Transaldolases. J. Biol. Chem. 276, 11055–11061. https://doi.org/10.1074/jbc.M008061200.

Shaw, P.D., Hager, L.P., 1961. VI. Chloroperoxidase: a component of the beta-ketoadipate chlorinase system. J. Biol. Chem. 236, 1626–1630. https://doi.org/10.1016/S0021-9258(19)63275-8.

Shevelkova, A.N., Ryabov, A.D., 1996. Irreversible inactivation of Caldariomyces fumago chloroperoxidase by hydrogen peroxide. A kinetic study in chloride and bromide system. Biochem. Mol. Biol Int 39, 665–670. https://doi.org/10.1080/15216549600201731.

Stütz, A.E., 1999. Iminosugars as Glycosidase Inhibitors. Wiley-VCH, Weinheim, Germany. 10.1002/3527601740.fmatter.

Sudar, M., Česnik, M., Clapés, P., Pohl, M., Vasić-Rački, Đ., Findrik Blažević, Z., 2021. A cascade reaction for the synthesis of D-fagomine precursor revisited: Kinetic insight and understanding of the system. N. Biotechnol. 63, 19–28. https://doi.org/10.1016/j.nbt.2021.02.004.

Sudar, M., Findrik, Z., Lozano, C., 2013a. Mathematical model for aldol addition catalyzed by two d-fructose-6-phosphate aldolases variants overexpressed in E. coli. J. Biotechnol. 167, 191–200. https://doi.org/10.1016/j.jbiotec.2013.07.008.

Sudar, M., Findrik, Z., Vasić-Rački, D., Clapés, P., Lozano, C., 2013b. Aldol addition of dihydroxyacetone to N-Cbz-3-aminopropanal catalyzed by two aldolases variants in microreactors. Enzyme Microb. Technol. 53, 38–45. https://doi.org/10.1016/j.enzmictec.2013.03.013.

Sudar, M., Findrik, Z., Vasić-Rački, Đ., Soler, A., Clapés, P., 2015. A new concept for production of (3S,4R)-6-[(benzyloxycarbonyl)amino]-5,6-dideoxyhex-2-ulose, a precursor of D -fagomine. RSC Adv. 5, 69819–69828. https://doi.org/10.1039/C5RA14414K.

Sugiyama, M., Hong, Z., Liang, P.-H., Dean, S.M., Whalen, L.J., Greenberg, W.A., Wong, C.-H., 2007. D-Fructose-6-phosphate aldolase-catalyzed one-pot synthesis of iminocyclitols. J. Am. Chem. Soc. 129, 14811–14817. https://doi.org/10.1021/ja073911i.

Szekrenyi, A., Soler, A., Garrabou, X., Guérard-Hélaine, C., Parella, T., Joglar, J., Lemaire, M., Bujons, J., Clapés, P., 2014. Engineering the Donor Selectivity of D-Fructose-6-Phosphate Aldolase for Biocatalytic Asymmetric Cross-Aldol Additions of Glycolaldehyde. Chem. - A Eur. J. 20, 12572–12583. https://doi.org/10.1002/chem.201403281.

Tadic, M., Kralj, S., Jagodic, M., Hanzel, D., Makovec, D., 2014. Magnetic properties of novel superparamagnetic iron oxide nanoclusters and their peculiarity under annealing treatment. Appl. Surf. Sci. 322, 255–264. https://doi.org/10.1016/j.apsusc.2014.09.181.

Taniguchi, S., Asano, N., Tomino, F., Miwa, I., 1998. Potentiation of glucose-induced insulin secretion by fagomine, a pseudo- sugar isolated from mulberry leaves. Horm. Metab. Res. 30, 679–683. https://doi.org/10.1055/s-2007-978957.

Toti, P., Petri, A., Gambicorti, T., Osman, A.M., Bauer, C., 2005. Kinetic and stability studies on the chloroperoxidase complexes in presence of tert-butyl hydroperoxide. Biophys. Chem. 113, 105–113. https://doi.org/10.1016/j.bpc.2004.08.003.

Whalen, L.J., Wong, C.H., 2006. Enzymes in organic synthesis: aldolase-mediated synthesis of iminocyclitols and novel heterocycles. Aldrichimica Acta 39, 63–71. https://doi.org/10.1002/chin.200729227.